

## Single Step Solution Processed GaAs Thin Films from GaMe<sub>3</sub> and 'BuAsH<sub>2</sub> Under Ambient Pressure

Sanjayan Sathasivam <sup>a</sup>, Ranga R. Arnepalli <sup>b</sup>, Davinder S. Bhachu,<sup>a</sup> Yao Lu <sup>a</sup>, John Buckeridge <sup>b</sup>, David O. Scanlon <sup>b,c</sup>, Bhaskar Kumar <sup>d</sup>, Kaushal K. Singh <sup>d</sup>, Robert J. Visser <sup>d</sup>, Christopher S. Blackman <sup>a</sup> and Claire J. Carmalt<sup>a\*</sup>

\*Corresponding author

<sup>a</sup>Materials Chemistry Centre, Department of Chemistry, University College London, 20 Gordon Street, London WC1H 0AJ, UK

E-mail: [c.j.carmalt@ucl.ac.uk](mailto:c.j.carmalt@ucl.ac.uk)

<sup>b</sup>Kathleen Lonsdale Materials Chemistry, University College London, Department of Chemistry, 20 Gordon Street, London, WC1H 0AJ, UK

<sup>c</sup>Diamond Light Source Ltd., Diamond House, Harwell Science and Innovation Campus, Didcot, Oxfordshire OX11 0DE, United Kingdom.

<sup>d</sup>Applied Materials Inc., 3225 Oakmead Village Drive, M/S 1240 P.O. Box 58039, Santa Clara, California 95052-8039, USA

Email: [robert\\_visser@amat.com](mailto:robert_visser@amat.com)

### Abstract

This article reports on the possibility of low cost GaAs formed under ambient pressure *via* a single step solution processed route from only readily available precursors, 'BuAsH<sub>2</sub> and GaMe<sub>3</sub>. The thin films of GaAs on glass substrates were found to have good crystallinity with crystallites as large as 150 nm and low contamination with experimental results matching well with theoretical density of states calculations. These results open up a route to efficient and cost-effective scale up of GaAs thin films with high material properties for widespread industrial use. Confirmation of film quality was determined using XRD, Raman, EDX mapping, SEM, HRTEM, XPS and SIMS. Thus the pathway to inexpensive high-quality GaAs films for photovoltaic and other optoelectronic applications has been laid.

## Introduction

Gallium arsenide (GaAs) is the most studied material of the III-V class of semiconductors; in fact it is second only to the ubiquitous Si as the most important semiconductor.<sup>1-3</sup> It has a direct band gap of 1.43 eV (at RT) and high optical absorption coefficient that enables it to be activated by much of the solar spectrum.<sup>2</sup> This coupled with its inherent high charge carrier mobilities permit it to achieve record-breaking solar conversion efficiencies (28.8%) and hence make excellent photovoltaic devices.<sup>4-7</sup> Furthermore it is also widely used in optoelectronics such as thin film transistors and radio frequency devices.<sup>8</sup> Owing to the current pace of development in the optoelectronic industry, Si based devices will soon struggle to keep up with demand for smaller, higher speed and more energy efficient equipment. GaAs has the potential to meet such commercial demands and not just be limited to military and space based applications, as currently. However, the widespread deployment of GaAs in commercial technology is limited by high production costs. The conventional methods to GaAs thin films involve the use of metal organic chemical vapor deposition (MOCVD) or molecular beam epitaxy (MBE) at high temperatures on expensive single crystal substrates (GaAs or Ge) under ultra high vacuum (UHV) conditions.<sup>9</sup>

Thus far, efforts to reduce the cost of GaAs film based technology have involved the use of alternative inexpensive substrates such as Si, Mo, glass and even plastics while using conventional deposition techniques under UHV conditions.<sup>10-12</sup> Furthermore, epitaxial lift-off, whereby GaAs films grown on single crystal wafers are removed and the wafer reused have been effective in reducing costs.<sup>9, 13-15</sup> However, issues with this method not only arise from the highly corrosive difficult to handle HF that is used to remove the sacrificial AlGaAs between the GaAs layers, but also from the high surface roughness that is imparted on the substrate which typically requires mechanical treatment to be reclaimed.<sup>13</sup>

This paper describes a method to circumvent high costs in the fabrication of quality GaAs thin films by ambient pressure deposition on inexpensive glass substrates through a solution-based route. Despite solution processed semiconductor thin films becoming more common in recent times (e.g. TiO<sub>2</sub> and *via* sol-gel dip or spin coating)<sup>16</sup> even in photovoltaic applications (perovskites, CIGS *via* spin coating or

spraying)<sup>17-19</sup> it has not been implemented for the synthesis of GaAs and other III-V materials.

Here we use a specialized form of CVD called aerosol assisted chemical vapor deposition (AACVD) for the fabrication of high quality GaAs thin films. AACVD is a solution based film synthesis technique that utilizes the advantages of solution processing methods such as deposition at atmospheric pressure and large area coverage along with the associated low cost and ease of use with the single step, high crystallinity and high purity films that are routinely achieved *via* MOCVD. Also, these solutions processed films presented below were easily tunable, for example, to achieve the required stoichiometry by simply changing the recipe of the solution. In AACVD a solution containing the desired precursor(s) is dissolved in a suitable solvent then atomised and transported under atmospheric pressure into a heated deposition chamber using a carrier gas. Using AACVD, a polycrystalline GaAs film was deposited in a single step using the commercially available precursors, <sup>4</sup>BuAsH<sub>2</sub> and GaMe<sub>3</sub> in a toluene solution. The film was fully characterized for its material properties to show that it was indeed possible to produce high quality GaAs films *via* a solution-based method. Also included is an XPS valence band study and comparison with density of state calculations that showed a good match between experimental and theoretical models for the deposited GaAs film.

## **Results and Discussion**

Polycrystalline GaAs thin films were grown on glass substrates held at 500 °C from a one-pot solution of <sup>4</sup>BuAsH<sub>2</sub> (5.5 mmol) and GaMe<sub>3</sub> (1.8 mmol) in 30 mL of toluene *via* the AACVD method. The films appeared grey/blue in colour and were well adhered to the substrate passing the Scotch<sup>TM</sup> tape test.

X-ray diffraction performed on the GaAs films show them to be in the expected cubic phase with peaks at 27.3°, 45.4° and 53.8° for the (111), (220) and (311) reflections respectively (Figure 1a). The Scherrer equation was applied to the XRD data to determine an estimate of the average crystallite size of 17 (±2) nm (see supporting information). Texture coefficient calculations indicate that the films have crystallographic preferred orientation in the (311) direction and a lack of orientation in the (220) direction with respect to the GaAs standard pattern (see supporting information). This is primarily due to the strain caused by interactions between the

film and the amorphous glass substrate, which is also the reason for the deviation in the lattice parameters. This phenomenon has been observed previously even for polycrystalline metal oxide systems grown on glass.<sup>20</sup> There was no deviation in unit cell volume from standard data for the deposited films. This was calculated by fitting a Le Bail model to the XRD pattern using GSAS and EXGUI programs (see supporting information).<sup>21</sup>

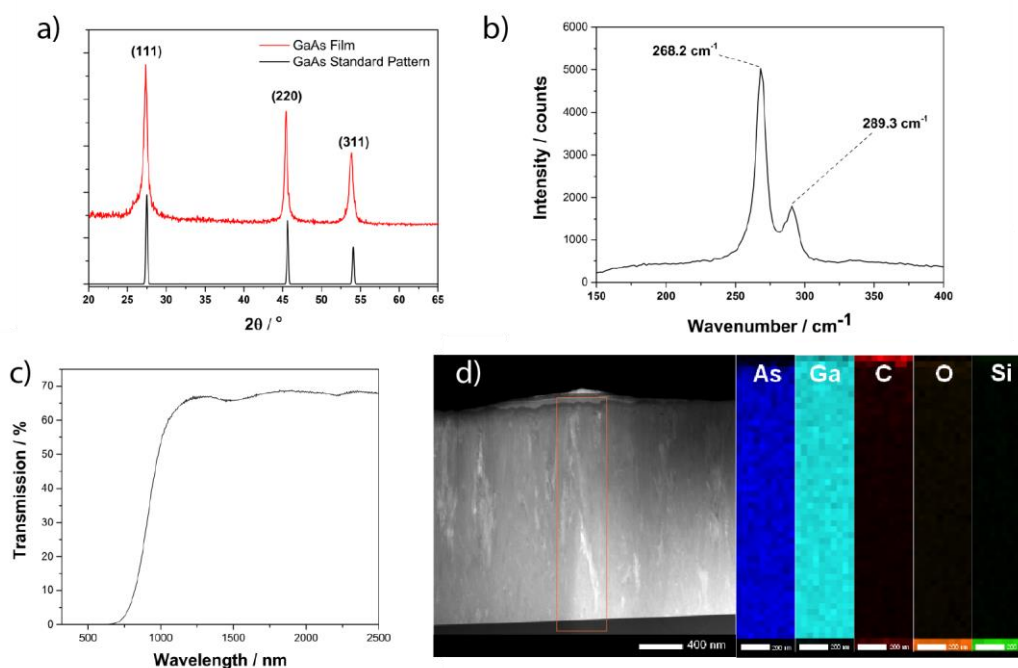


**Figure 1:** a) The powder XRD pattern for the polycrystalline GaAs film grown at 500 °C from a toluene solution of  $t\text{-BuAsH}_2$  and  $\text{GaMe}_3$ . Standard GaAs pattern is also shown. b) Raman spectrum showing both the LO (at  $289.3\text{ cm}^{-1}$ ) and TO (at  $268.2\text{ cm}^{-1}$ ) peaks. c) UV-vis spectrum showing the transmittance of the film. d) EDX mapping from the surface of the AACVD grown film through the bulk to the substrate. The lack of colour (blue for As, turquoise for Ga, red for C, orange for O and green for Si) indicates the absence of the element in that region.

Figure 1b shows the Raman scattering data from the GaAs film with the longitudinal optical (LO) phonon mode observed at  $289.3\text{ cm}^{-1}$  and the transverse optical (TO) mode at  $268.2\text{ cm}^{-1}$ . These values compare well with literature although there is a small red shift in the peak positions which is indicative of tensile strain of the lattice.<sup>22-23</sup>

The UV-vis spectrum of the film shown in Figure 1c is typical of what is expected for GaAs, transmittance is high (ca. 70%) in the near infrared region. The film absorbs in

the visible region with the direct band gap calculated *via* the Tauc method to be 1.53 eV, slightly blue shifted compared to literature findings.<sup>24-25</sup>

Energy dispersive X-ray spectroscopy (EDX) showed the films to have a Ga to As ratio of 1:1 with no contaminants other than the expected O and C. This is primarily due to the clean film synthesis route involving a solution of only  $t\text{-BuAsH}_2$ ,  $\text{GaMe}_3$  and toluene. Further evidence for the purity of the film is shown by EDX mapping (Figure 1c). The mapping was carried out on a region *ca.* 400 nm wide from the surface of the film to the glass substrate, this revealed that the As and Ga levels were in equal measure as indicated by the homogeneity of the blue and turquoise colouration in Figure 1c. Also, the lack of colour in the C (red), O (orange) and Si (green) graphs indicates the absence or below detection limit levels of these elements in the bulk of the film. The O and C contaminants detected were only on the surface of the film.

Analysis of the film surface morphology *via* scanning electron microscopy (SEM) show it to consist of closely packed domes some of which are 100-150 nm wide (Figure 2 and b). The sizes of these domes are much smaller than what can be achieved on lattice matched single crystal GaAs or Ge substrates that can be as large as a few micrometers. This is due to the templating effect lattice match substrates have on the growing film, evidently this templating does not take place when the substrate is amorphous. Thus resulting in smaller crystallites/grains as observed here. Typically smaller crystallites/grains would have a negative impact on device properties due to grain boundaries acting as charge carrier recombination and scattering sites (leading to reduced carrier mobility).

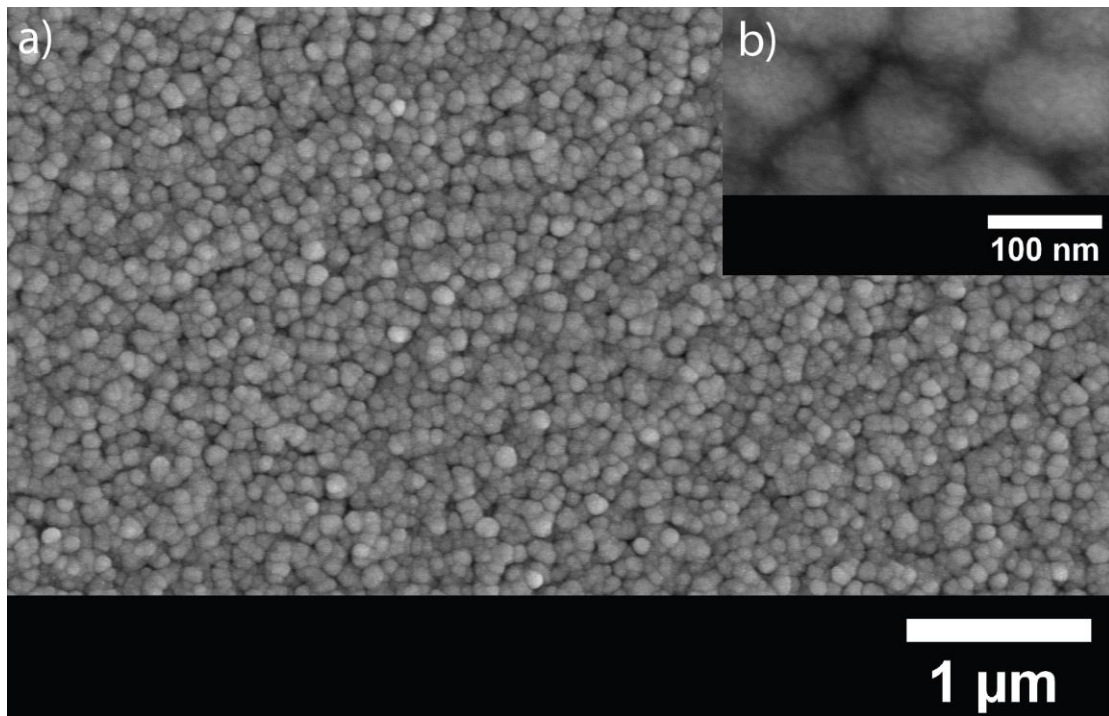


**Figure 2:** a) SEM micrograph of the GaAs film grown *via* AACVD at 500 °C. The morphology consists of densely packed domes roughly 100 -150 nm in diameter as shown in inset (b).

High-resolution transmission electron spectroscopy (HRTEM) data shown in Figure 3 reveal the polycrystalline nature of the film with highly crystalline grains as indicated by the well-defined lattice fringes (Figure 3b). There is a variation in the grain size from the surface to the bottom of the film close to the substrate (Figure 3c and d). As expected the region close to the substrate is made up of smaller grains (average 30 nm) due to film growth taking place on an amorphous substrate, as film thickness increases the grains become larger (average 66 nm) because the layers beneath act as crystalline templates facilitating a more ordered and hence more crystalline growth. Some grains analysed were as large as 150 nm in width.

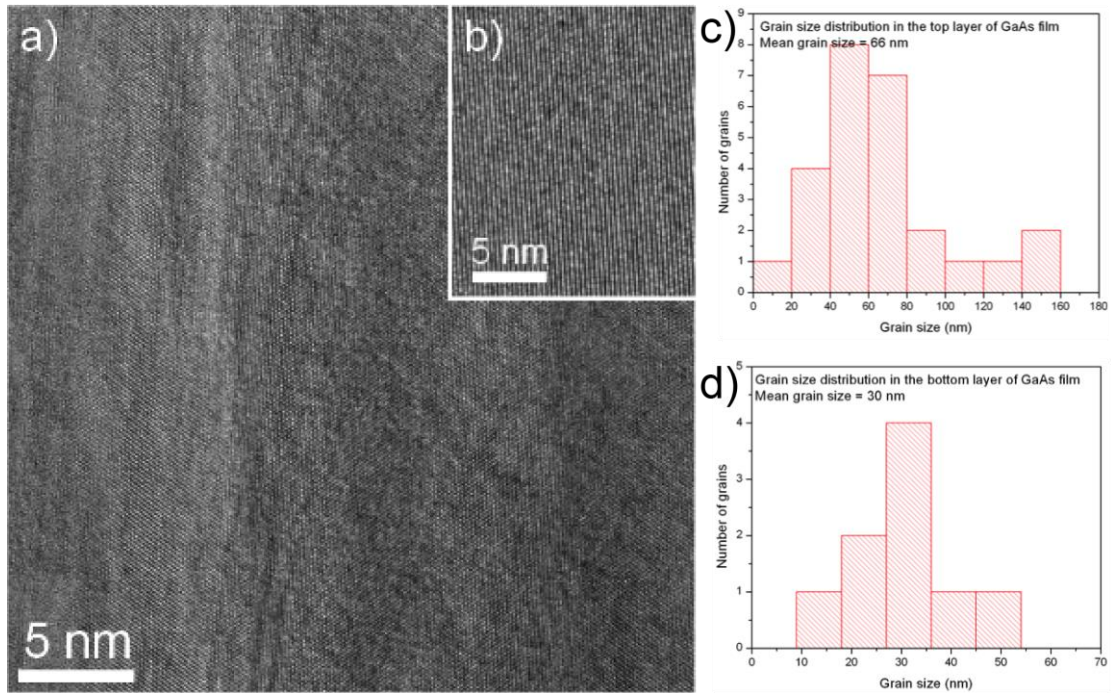


**Figure 3: a) HRTEM of the GaAs films grown at 500 °C under ambient pressure shows good crystallinity with well-separated lattice fringes (b). c) And d) show the grain size distribution near the surface and bottom (close to the substrate), respectively, as determined *via* HRTEM. The grains are larger near the surface due to templating effects.**

In addition, darkfield and lightfield cross sectional images (Figure 4a and b respectively) of the film show good crystallinity perpendicular to the substrate indicating columnar film growth. This, coupled with the large grain sizes (Figure 3c), is advantageous as it reduces grain boundaries and hence decreases charge carrier recombination that can be detrimental to photovoltaic and other electronic devices due to reduced fill factor and open circuit voltage and efficiency.<sup>26</sup>

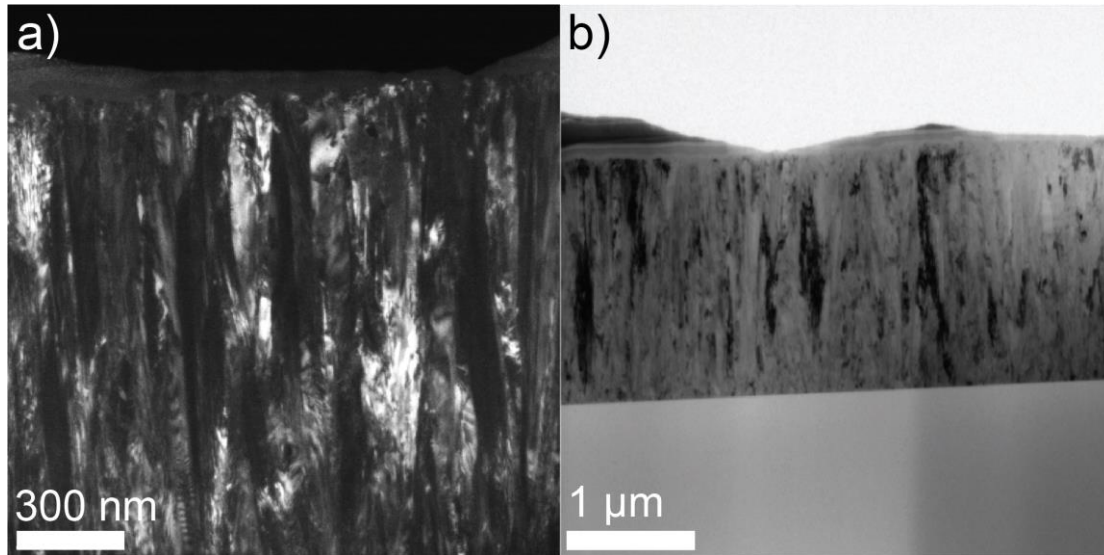


**Figure 4: The darkfield (a) and lightfield (b) show the columnar nature of the film growth, reducing grain boundaries in the vertical direction.**

X-ray photoelectron spectroscopy (XPS) measurements showed the presence of Ga, As, O and C on the surface. Deconvolution of the As 3d peak revealed an As 3d<sub>5/2</sub> peak at 40.5 eV matching As bound to Ga, the corresponding Ga in GaAs showed a 3d<sub>5/2</sub> peak at 19.3 eV.<sup>27</sup> As and Ga oxide peaks were also present in both the 3d spectra due to the native oxide layer that is typical of GaAs.<sup>27</sup> However upon sputtering the surface these peaks disappeared corresponding well with what was observed from the EDX mapping experiments (Figure 1c). XPS depth profiling (Figure 5a - d) also showed that after 1000 seconds of etching the film was void of both carbon and oxygen contaminants (Figure 5c and d).

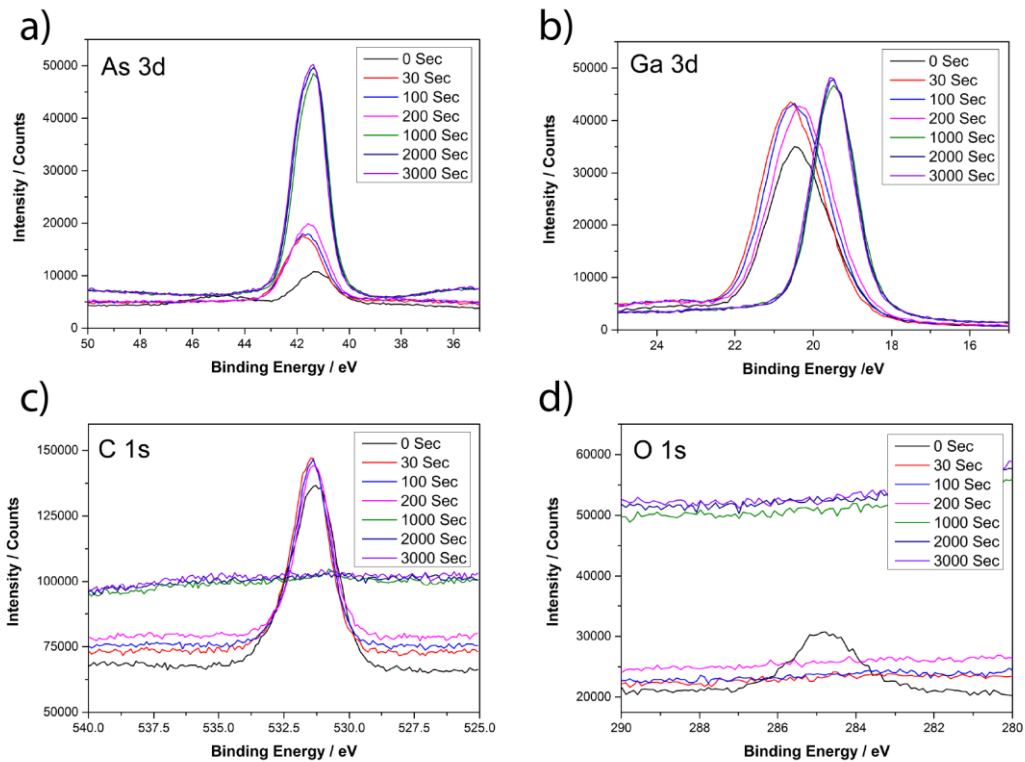


**Figure 5: XPS depth profiling study showing a) As 3d, b) Ga 3d, c) O 1s and d) C 1s. C and O are mainly surface bound**

Further analysis for low concentration of C, O and Si contaminants in the bulk of the film was carried out using depth profiling secondary ion mass spectroscopy (SIMS) (Figure 6). As was used as the reference matrix element. In general the signals for C and O are low in the bulk of the film at below  $3 \times 10^{19}$  and  $5 \times 10^{20}$  atoms/cm<sup>3</sup> respectively. Due to the relatively low temperature of the fabrication, Si diffusion into GaAs film from the glass substrate is minimized (secondary ion intensity was in the order of  $\times 10^1$  counts per second) even near the film-substrate junction. The SIMS data also correspond well with the observations made using EDX mapping and XPS depth profiling analysis.

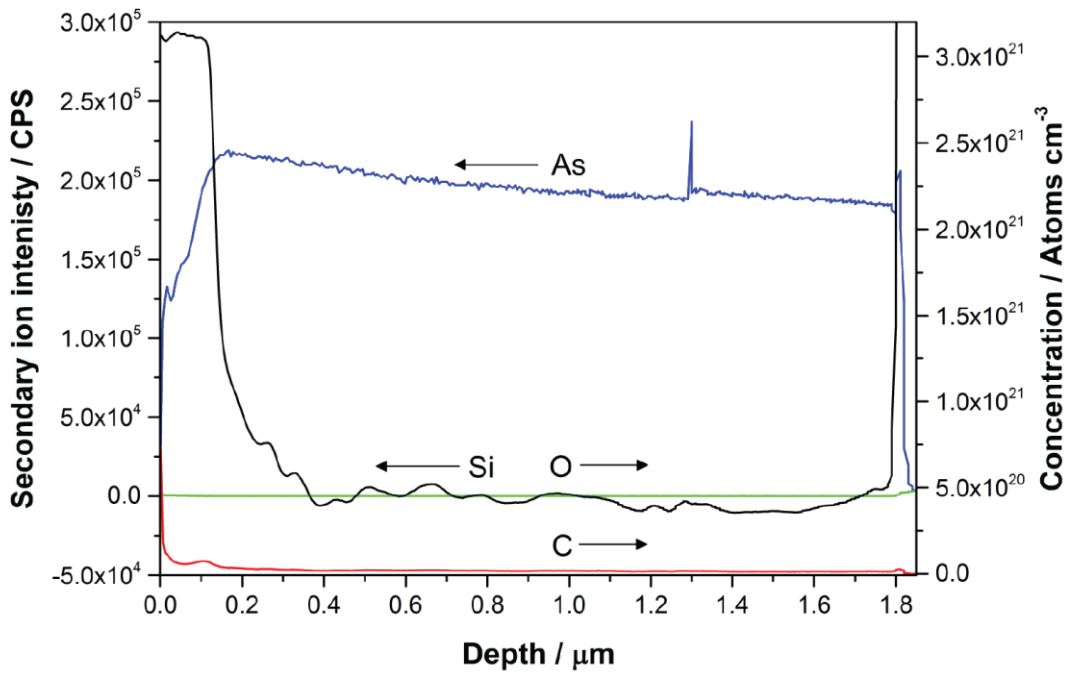


**Figure 6:** SIMS analysis showing the C and O levels on the surface and the bulk of the film, SIMS also confirmed that there was no contamination from Si in the film. SIMS data matches well with EDX mapping and XPS analysis.

The valence band spectrum shown in Figure 7 for the film matches well with literature observations and (as presented) with our calculated density of states simulations. In particular, the peak positions at binding energies 2.2 eV, 7 eV and 12.0 eV, that originate from outermost atomic s and p orbitals of Ga and As, are in excellent agreement with our hybrid density functional calculations and literature reports. Furthermore, the shoulder at 3 eV on the peak at centered at 2.2 eV for the GaAs was also observed in the simulated spectrum and literature findings. Conversely the small bump observed at 9.5 eV in the experimental data was not observed in the calculated plot. This discrepancy may be due to the XPS valence band analysis being surface sensitive whereas the DOS calculations are based on bulk GaAs.

The Fermi level in GaAs, as for typical n type semiconductors, is restrained near the mid way point between the valence and conduction band by negatively charged surface states. Hence the Fermi level lies lower than expected giving rise to a band edge near 0 eV.<sup>28</sup>

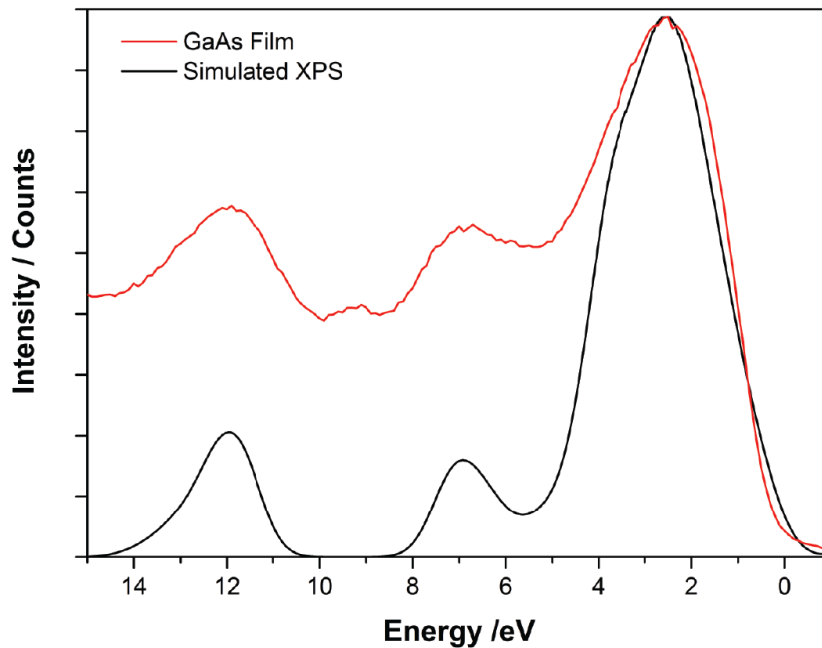


**Figure 7: XPS valence band of the GaAs film as compared to a stimulated DOS model.**

## **Conclusion**

In conclusion, we demonstrate the possibility of an inexpensive and high throughput method to GaAs from readily available precursors in a toluene solution for photovoltaic applications. The use of the solution based AACVD technique enables high quality GaAs layers with good crystallinity (grain size up to 150 nm) on non-lattice matched inexpensive substrates, low contamination levels (O and C only surface bound). The film was also stoichiometric without the need for a great excess of  $t\text{-BuAsH}_2$ .

## **Experimental**

*Caution! Trimethylgallium and tertbutylarsine are pyrophoric substances that ignite spontaneously in air and therefore must be handled under an inert atmosphere. Tertbutylarsine is highly toxic and must be handled with care. All experiments must be carried out in a fume cupboard. Post deposition the films are air/moisture stable and safe to handle, all reactive species leave via the exhaust during the AACVD process.*

Trimethylgallium (99.999%) was used as received from SAFC Hitech Ltd. Tertbutylarsine (99.999%) was purchased from and used as received from Dockweiler Chemicals. Toluene was purchased from Alfa Aesar and stored under alumina columns and dried with Anhydrous Engineering equipment.

To form the precursor solution,  $t\text{BuAsH}_2$  (0.74 g, 5.5 mmol) was dissolved in toluene (15 mL) at  $-78\text{ }^\circ\text{C}$ .  $\text{GaMe}_3$  (0.21 g, 1.8 mmol) was dissolved in toluene (15 mL) at  $-78\text{ }^\circ\text{C}$ . The  $t\text{BuAsH}_2$  in toluene solution was added drop wise to the  $\text{GaMe}_3$ /toluene and allowed to reach room temperature under stirring before deposition was carried out at  $500\text{ }^\circ\text{C}$ .

Depositions were carried out under nitrogen in a cold wall reactor. The precursor mixture was placed in a glass bubbler and an aerosol mist was created using a piezoelectric device (Vicks ultrasonic humidifier, model number: 4022167500175) placed below the bubbler containing  $t\text{BuAsH}_2$  (5.5 mmol) and  $\text{GaMe}_3$  (1.8 mmol) in 30 mL of toluene. The precursor flow was kept at  $0.5\text{ L}\cdot\text{min}^{-1}$ . The glass substrate was Corning glass (size  $15\text{ cm} \times 4\text{ cm} \times 0.1\text{ cm}$ ) and was cleaned using distilled water, isopropanol and acetone. A top plate was suspended 0.5 cm above the glass substrate to ensure a laminar flow. The substrate temperature was kept at  $500\text{ }^\circ\text{C}$ . Deposition time was 60 minutes. After the deposition the bubblers were closed and the substrates were cooled under a flow of nitrogen. At the end of the deposition the nitrogen flow through the aerosol was diverted and only nitrogen passed over the substrate. The glass substrate was allowed to cool with the graphite block to room temperature before it was removed. Coated substrates were handled and stored in air.

X-ray diffraction (XRD) was carried out using a microfocus Bruker GAADS powder X-ray diffractometer with a monochromated  $\text{Cu K}\alpha$  ( $1.5406\text{ \AA}$ ) source. X-ray photoelectron spectroscopy (XPS) was carried out using a Thermo Scientific *K*-Alpha instrument with monochromatic  $\text{Al-K}\alpha$  source to identify the oxidation state and chemical constituents. High-resolution scans were done for the Ga (3d), As (3d), O (1s) and C (1s) at a pass energy of 40 eV. The Ga atom% was derived from the  $\text{Ga-K}\alpha$  line (9242.9 eV) and the As atom% derived from the  $\text{As-L}\alpha$  (10532.0 eV). The peaks were modeled using CasaXPS software with binding energies calibrated to carbon (284.5 eV). Additional XPS measurements were carried out by Applied Materials, Santa Clara, Ca, USA. SEM images were taken on a JOEL JSM-6301F Field

Emission instrument with acceleration voltage of 5 kV. Images were captured using SEMAfore software. EDX was measured on a JOEL JSM-6301F Field Emission instrument with acceleration voltage of 20 kV, the Ga atom% was derived from Ga- $K_{\alpha}$  line (9243 eV) and the As atom% derived from the As  $K_{\alpha}$  line (1053 eV). For both SEM and EDX samples were cut to 10 mm x 10 mm coupons and coated with a fine layer of gold (SEM) and carbon (EDX) to avoid charging. HRTEM and EDX mapping was carried out on Titan 80-300 TEM with EDX at CAMCOR service at the University of Oregon. SIMS was carried out by Evans analytical group, Santa Clara, California.

Density functional theory (DFT) calculations were performed using the VASP<sup>29,30</sup> code, with the projector-augmented wave approach<sup>31</sup> used to describe the interaction between the core (Ga:[Ar] and As:[Ar]) and valence electrons. The calculations implemented the screened hybrid functional as proposed by Heyd, Scuseria, and Ernzerhof (HSE).<sup>32</sup> To accurately reproduce the experimentally known band gap of GaAs of 1.52 eV at 0 K<sup>33</sup>, an exchange value of 30%, was utilized. The HSE approach consistently produces structural and band gap data that are more accurate than standard density functional approaches, such as the local density approximation (LDA) or the generalized gradient approximation (GGA).<sup>34-39</sup> A cut-off value of 600 eV and a k-point mesh of 8x8x8 centred on the  $\Gamma$  point, were found to be sufficient. All calculations were deemed to be converged when the forces on all atoms were less than 0.01 eV  $\text{\AA}^{-1}$ . Spin orbit effects were included in all calculations.

The minimized lattice parameters were 5.65  $\text{\AA}$ , with a band gap of 1.52 eV and a spin orbit splitting of 361 meV, in excellent agreement with low temperature experiments.<sup>33, 40-41</sup> The PEDOS contributions were weighted by the known x-ray photoionization cross section<sup>42</sup> of their respective atoms and were then summed, resulting in the total VB-DOS. The weighting was performed to accurately represent the processes that contributed to the experimental XPS data.

## **Acknowledgements**

C.J.C and S.S. would like to thank Applied Materials Inc, USA for funding the project. Dr. Ben Schmiege for useful discussion, Mr. Kevin Reeves for assistance with SEM

imaging and Dr. Ghazel Saheli for XPS depth profiling. J.B. and D.O.S. acknowledge access to the ARCHER supercomputer *via* membership of the UK's HPC Materials Chemistry Consortium, which is funded by EPSRC grant EP/L000202.

### **Author contributions**

S.S designed/carried out the experiments, performed sample characterization (all but HRTEM and SIMS), analyzed the results and wrote the manuscript. R.R.A contributed to the design of experiments and sample characterization. D.S.B analyzed the XPS valence band results. S.S and Y.L made the figures and organized the manuscript. J.B and D.O.S performed the theoretical calculations and contributed to writing of the manuscript. C.S.B and C.J.C supervised S.S, D.S.B and Y.L and were involved in the design of experiments, editing of the manuscript and discussions throughout the work. R.R.A, B.K, K.K.S and R.J.V were involved in the design of experiments and discussions throughout the work.

## References

1. Bett, A. W.; Dimroth, F.; Stollwerck, G.; Sulima, O. V., III-V compounds for solar cell applications. *Applied Physics A* **1999**, *69* (2), 119-129.
2. Blakemore, J., Semiconducting and other major properties of gallium arsenide. *J. Appl. Phys.* **1982**, *53* (10), R123-R181.
3. Ritenour, A. J.; Boucher, J. W.; DeLancey, R.; Greenaway, A. L.; Aloni, S.; Boettcher, S. W., Doping and electronic properties of GaAs grown by close-spaced vapor transport from powder sources for scalable III-V photovoltaics. *Energy & Environmental Science* **2015**, *8* (1), 278-285.
4. Green, M. A.; Emery, K.; Hishikawa, Y.; Warta, W.; Dunlop, E. D., Solar cell efficiency tables (Version 45). *Progress in Photovoltaics: Research and Applications* **2015**, *23* (1), 1-9.
5. Han, N.; Yang, Z.-x.; Wang, F.; Dong, G.; Yip, S.; Liang, X.; Hung, T. F.; Chen, Y.; Ho, J. C., High-Performance GaAs Nanowire Solar Cells for Flexible and Transparent Photovoltaics. *ACS Applied Materials & Interfaces* **2015**, *7* (36), 20454-20459.
6. Ritenour, A. J.; Cramer, R. C.; Levinrad, S.; Boettcher, S. W., Efficient n-GaAs Photoelectrodes Grown by Close-Spaced Vapor Transport from a Solid Source. *ACS Applied Materials & Interfaces* **2012**, *4* (1), 69-73.
7. Kayes, B. M.; Nie, H.; Twist, R.; Spruytte, S. G.; Reinhardt, F.; Kizilyalli, I. C.; Higashi, G. S. In *27.6% Conversion efficiency, a new record for single-junction solar cells under 1 sun illumination*, 2011; IEEE: pp 000004-000008.
8. Schwierz, F.; Liou, J. J., RF transistors: Recent developments and roadmap toward terahertz applications. *Solid-State Electron.* **2007**, *51* (8), 1079-1091.
9. Yoon, J.; Jo, S.; Chun, I. S.; Jung, I.; Kim, H.-S.; Meitl, M.; Menard, E.; Li, X.; Coleman, J. J.; Paik, U., GaAs photovoltaics and optoelectronics using releasable multilayer epitaxial assemblies. *Nature* **2010**, *465* (7296), 329-333.
10. Jones, K.; Al-Jassim, M.; Hasoon, F.; Venkatasubramanian, R. In *The morphology and microstructure of thin-film GaAs on Mo substrates*, AIP Conf. Proc., IOP INSTITUTE OF PHYSICS PUBLISHING LTD: **1998**; pp 531-536.
11. Fischer, R.; Morkoc, H.; Neumann, D.; Zabel, H.; Choi, C.; Otsuka, N.; Longerbone, M.; Erickson, L., Material properties of high - quality GaAs epitaxial layers grown on Si substrates. *J. Appl. Phys.* **1986**, *60* (5), 1640-1647.
12. Sathasivam, S.; Arnepalli, R. R.; Kumar, B.; Singh, K. K.; Visser, R. J.; Blackman, C. S.; Carmalt, C. J., Solution Processing of GaAs Thin Films for Photovoltaic Applications. *Chem. Mater.* **2014**, *26* (15), 4419-4424.
13. Cheng, C.-W.; Shiu, K.-T.; Li, N.; Han, S.-J.; Shi, L.; Sadana, D. K., Epitaxial lift-off process for gallium arsenide substrate reuse and flexible electronics. *Nat Commun* **2013**, *4*, 1577.
14. Yablonovitch, E.; Gmitter, T.; Harbison, J.; Bhat, R., Extreme selectivity in the lift - off of epitaxial GaAs films. *Appl. Phys. Lett.* **1987**, *51* (26), 2222-2224.
15. Sathasivam, S.; Arnepalli, R. R.; Singh, K. K.; Visser, R. J.; Blackman, C. S.; Carmalt, C. J., A solution based route to GaAs thin films from As(NMe<sub>2</sub>)<sub>3</sub> and GaMe<sub>3</sub> for solar cells. *RSC Advances* **2015**, *5* (16), 11812-11817.
16. Pasquarelli, R. M.; Ginley, D. S.; O'Hayre, R., Solution processing of transparent conductors: from flask to film. *Chem. Soc. Rev.* **2011**, *40* (11), 5406-5441.
17. Green, M. A.; Ho-Baillie, A.; Snaith, H. J., The emergence of perovskite solar cells. *Nat Photon* **2014**, *8* (7), 506-514.

18. Liu, D.; Kelly, T. L., Perovskite solar cells with a planar heterojunction structure prepared using room-temperature solution processing techniques. *Nat Photon* **2014**, *8* (2), 133-138.
19. Kaelin, M.; Rudmann, D.; Tiwari, A., Low cost processing of CIGS thin film solar cells. *Solar Energy* **2004**, *77* (6), 749-756.
20. Ghosh, R.; Basak, D.; Fujihara, S., Effect of substrate-induced strain on the structural, electrical, and optical properties of polycrystalline ZnO thin films. *J. Appl. Phys.* **2004**, *96* (5), 2689-2692.
21. Toby, B. H., EXPGUI, a graphical user interface for GSAS. *J. Appl. Crystallogr.* **2001**, *34* (2), 210-213.
22. Campbell, I. H.; Fauchet, P. M., The effects of microcrystal size and shape on the one phonon Raman spectra of crystalline semiconductors. *Solid State Commun.* **1986**, *58* (10), 739-741.
23. Abstreiter, G.; Bauser, E.; Fischer, A.; Ploog, K., Raman spectroscopy—A versatile tool for characterization of thin films and heterostructures of GaAs and Al<sub>x</sub>Ga<sub>1-x</sub>As. *Applied physics* **1978**, *16* (4), 345-352.
24. Tauc, J.; Grigorovici, R.; Vancu, A., Optical Properties and Electronic Structure of Amorphous Germanium. *physica status solidi (b)* **1966**, *15* (2), 627-637.
25. Tauc, J., Optical properties and electronic structure of amorphous Ge and Si. *Mater. Res. Bull.* **1968**, *3* (1), 37-46.
26. Liang, D.; Kang, Y.; Huo, Y.; Chen, Y.; Cui, Y.; Harris, J. S., High-Efficiency Nanostructured Window GaAs Solar Cells. *Nano Lett.* **2013**, *13* (10), 4850-4856.
27. Grunthaner, F. J.; Grunthaner, P. J.; Vasquez, R. P.; Lewis, B. F.; Maserjian, J.; Madhukar, A., Local atomic and electronic structure of oxide/GaAs and SiO<sub>2</sub>/Si interfaces using high - resolution XPS. *Journal of Vacuum Science & Technology* **1979**, *16* (5), 1443-1453.
28. King, P. D. C.; Veal, T. D., Conductivity in transparent oxide semiconductors. *J. Phys. Condens. Matter* **2011**, *23* (33).
29. Kresse, G.; Furthmüller, J., Efficiency of ab-initio total energy calculations for metals and semiconductors using a plane-wave basis set. *Computational Materials Science* **1996**, *6* (1), 15-50.
30. Kresse, G.; Hafner, J., Ab initio molecular-dynamics simulation of the liquid-metal–amorphous-semiconductor transition in germanium. *Physical Review B* **1994**, *49* (20), 14251.
31. Blöchl, P. E., Projector augmented-wave method. *Physical Review B* **1994**, *50* (24), 17953.
32. Krukau, A. V.; Vydrov, O. A.; Izmaylov, A. F.; Scuseria, G. E., Influence of the exchange screening parameter on the performance of screened hybrid functionals. *The Journal of chemical physics* **2006**, *125* (22), 224106.
33. Schultheis, L.; Köhler, K.; Tu, C. W., Energy shift and line broadening of three-dimensional excitons in electric fields. *Physical Review B* **1987**, *36* (12), 6609-6612.
34. Allen, J. P.; Scanlon, D. O.; Watson, G. W., Electronic structure of mixed-valence silver oxide AgO from hybrid density-functional theory. *Physical Review B* **2010**, *81* (16), 161103.
35. Burbano, M.; Scanlon, D. O.; Watson, G. W., Sources of conductivity and doping limits in CdO from hybrid density functional theory. *J. Am. Chem. Soc.* **2011**, *133* (38), 15065-15072.

36. Kehoe, A. B.; Scanlon, D. O.; Watson, G. W., Role of Lattice Distortions in the Oxygen Storage Capacity of Divalently Doped CeO<sub>2</sub>. *Chem. Mater.* **2011**, *23* (20), 4464-4468.
37. Scanlon, D. O.; Walsh, A.; Watson, G. W., Understanding the p-Type Conduction Properties of the Transparent Conducting Oxide CuBO<sub>2</sub>: A Density Functional Theory Analysis. *Chem. Mater.* **2009**, *21* (19), 4568-4576.
38. Scanlon, D. O.; Watson, G. W., Undoped n-Type Cu<sub>2</sub>O: Fact or Fiction? *The Journal of Physical Chemistry Letters* **2010**, *1* (17), 2582-2585.
39. Scanlon, D. O.; Watson, G. W., Band gap anomalies of the ZnM<sub>2</sub>IIIIO<sub>4</sub> (MIII = Co, Rh, Ir) spinels. *Phys. Chem. Chem. Phys.* **2011**, *13* (20), 9667-9675.
40. Kozhevnikov, M.; Ashkinadze, B. M.; Cohen, E.; Ron, A., Low-temperature electron mobility studied by cyclotron resonance in ultrapure GaAs crystals. *Physical Review B* **1995**, *52* (24), 17165-17171.
41. Shantharama, L.; Adams, A.; Ahmad, C.; Nicholas, R., The kp interaction in InP and GaAs from the band-gap dependence of the effective mass. *Journal of Physics C: Solid State Physics* **1984**, *17* (25), 4429.
42. Yeh, J. J.; Lindau, I., Atomic subshell photoionization cross sections and asymmetry parameters:  $1 \leq Z \leq 103$ . *Atomic Data and Nuclear Data Tables* **1985**, *32* (1), 1-155.